Electronic Supplementary Material (ESI) for Chemical Communications.
This journal is © The Royal Society of Chemistry 2020

Electronic Supplementary Information

Teaching Old Indicators Even More Tricks: Binding Affinity Measurements with the Guest-Displacement Method (GDA)

Stephan Sinn,*[a] Joana Krämer,[a] and Frank Biedermann*[a]

a Dr. S. Sinn, MSc. J. Krämer, Dr. F. Biedermann
Institute of Nanotechnology (INT)
Karlsruhe Institute of Technology (KIT),
Hermann-von-Helmholtz Platz 1, 76344 Eggenstein-Leopoldshafen
Germany
E-Mail: stephan.sinn@kit.edu
E-Mail:frank.biedermann@kit.edu

1 Table of Contents

2 General Information

2.1 Abbreviations

H	host
G	guest
D	indicator dye
DBA	direct-binding assay
IDA	indicator-displacement assay
GDA	guest-displacement assay
CB8	cucurbit[8]uril
CB7	cucurbit[7]uril
β-CD	β-cyclodextrin
HSA	human serum albumin (fatty acid free)
TNS	2-p-toluidinylnaphthalene-6-sulfonate (2,6-TNS)
BE	berberine
MDAP	*N,N'*-dimethyl diazapyrene
MV	methyl viologen (doubly oxidized form, 2+)
AdOH	1-adamantanol
EtOH	ethanol
n-BuOH	*n*-butanol
t-BuOH	*t*-butanol
i-PrOH	*iso*-propanol
PBZ	phenylbutazone
PB	sodium phosphate buffer
PBS	phosphate buffered saline (137 mM NaCl, 2.7 mM KCl, 10 mM Na_2HPO_4 and 2 mM KH_2PO_4 dissolved in water)
NMR	nuclear magnetic resonance
λ	wavelength
ε	molar extinction coefficient
I	observable signal (fluorescence intensity)

2.2 Solubility

Table S1: Solubility of selected guests in water

compound	solubility in water	reference
ethanol	miscible	-
iso-propanol	miscible	-
n-butanol	miscible	-
t-butanol	miscible	-
adamantane	285 µM	[1]
1-adamantanol	soluble (> 2 mM)	[2]
PBZ (aq. solution)	145 µM	[3]
nortestosterone	810 µM	[4]
testosterone	114 µM	[4]
prednisolone	483 µM	[4]
estradiol	9 µM	[4]
progesterone	33 µM	[4]
warfarin (aq. solution)	55.1 µM	[5]
berberine chloride	13.2 mM	[6]
methyl viologen	2.50 M	[7]
TNS	> 4.0 mM	this work

2.3 Photophysical properties

Table S2: Photophysical properties of used dyes and corresponding host:dye complexes.

dye	host	λ_{abs}^{max} / nm[a]	λ_{em}^{max} / nm[b]
TNS	–	316	404
	CB7	322	398
	β-CD	316	463
BE	–	432	540[c]
	CB7	430	500
	CB8	425	532
MDAP	–	416	425
	CB7	423	431
MPCP	–	335	535
	CB8	342	542
warfarin[d]	–	308	402
	HSA	308	391

If not stated differently all measurements were conducted in deionized water at 25°C. [a] maximum of the lowest-energy band. [b] maximum of the highest-energy band. [c] almost no emission signal detectable [d] measured in PBS.

2.4 Experimental details

All solvents were used as received from Aldrich or Fluka without any further purification. All chemicals were purchased and used as received. ^{1}H NMR spectra were recorded on a Bruker Avance 500 spectrometer. The ^{1}H NMR chemical shifts (δ) are given in ppm and refer to residual protons on the corresponding deuterated solvent. All deuterated solvents were used as received without any further purification. All coupling constants (J) are given in Hertz (Hz).

Absorption spectra were measured on a Jasco V-730 double-beam UV–VIS spectrophotometer and baseline corrected. Steady-state emission spectra and time resolved emission profiles were recorded on a Jasco FP-8300 fluorescence spectrometer equipped with a 450 W xenon arc lamp, double-grating excitation, emission monochromators. Emission spectra were corrected for source intensity (lamp and grating) and the emission spectral response (detector and grating) by standard correction curves. For spectral recording the automatic filter change of the FP-8300 was applied in order to exclude second order diffraction artefacts. Titration curves were recorded by a Jasco FP-8300 fluorescence spectrometer where the titration was either performed manually or by an ATS-827 automatic titration unit filled with the appropriate compound (host/guest) and subsequently corrected for dilution. All titration experiments were carried out at T=25°C by using a water thermostated cell holder STR-812, while the cuvettes were equipped with a stirrer allowing rapid mixing.. For UV-Vis absorption experiments UV plastic cuvettes with a light path of 10 mm and dimensions of 10x10 mm from Brand with a spectroscopic cut-off at 240 nm were utilized. For fluorescence-based titration experiments PMMA cuvettes with a light path of 10 mm and dimensions of 10x10 mm from Brand with a spectroscopic cut-off at 300 nm were utilized.

3 Mathematical Equations for Thermodynamic Assay

3.1 Direct–Binding Assay (DBA)

$$H + D \rightleftarrows HD \quad \text{Eq. S1}$$

$$K_a^{HD} = \frac{[HD]}{[H][D]} \quad \text{Eq. S2}$$

$$[H]_0 = [HD] + [H] \quad \text{Eq. S3}$$

$$[D]_0 = [HD] + [D] \quad \text{Eq. S4}$$

$$I_c = I^0 + I^{HD} \cdot [HD] + I^D \cdot [D] \quad \text{Eq. S5}$$

[H] – host concentration at equilibrium, $[H]_0$ – initial host concentration,
[D] – dye concentration at equilibrium, $[D]_0$ – initial dye concentration,
[HD] – host⊃dye concentration at equilibrium,
K_a^{HD} – binding constant of host⊃dye (HD) complex,
I^0 – background signal, I^{HD} – signal from host⊃dye (HD) complex, I^D – signal from free dye (D),
I_c – observable signal as a function of concentration

3.2 Guest–Displacement Assay (GDA)

$$HG + D \rightleftarrows HD + G \qquad HG + 2D \rightleftarrows HD_2 + G$$ Eq. S6

$$H + D \rightleftarrows HD \qquad H + 2D \rightleftarrows HD_2$$ Eq. S7

$$H + G \rightleftarrows HG$$ Eq. S8

$$K_a^{HD} = \frac{[HD]}{[H][D]} \qquad K_a^{HD_2} = \frac{[HD_2]}{[H][D]^2}$$ Eq. S9

$$K_a^{HG} = \frac{[HG]}{[H][G]}$$ Eq. S10

$$[H]_0 = [HD] + [H] + [HG] \qquad [H]_0 = [HD_2] + [H] + [HG]$$ Eq. S11

$$[D]_0 = [HD] + [D] \qquad [D]_0 = 2[HD_2] + [D]$$ Eq. S12

$$[G]_0 = [HG] + [G]$$ Eq. S13

$$I_c = I^0 + I^{HD} \cdot [HD] + I^D \cdot [D] \qquad I_c = I^0 + I^{HD_2} \cdot [HD_2] + I^D \cdot [D]$$ Eq. S14

[H] – host concentration at equilibrium, $[H]_0$ – initial host concentration,
[D] – dye concentration at equilibrium, $[D]_0$ – initial dye concentration,
[G] – guest concentration at equilibrium, $[G]_0$ – initial guest concentration,
[HD] – host⊃dye concentration at equilibrium,
K_a^{HD} – binding constant of host⊃dye (HD) complex,
$[HD_2]$ – host⊃dye$_2$ concentration at equilibrium,
$K_a^{HD_2}$ – binding constant of host⊃dye$_2$ (HD_2) complex,
[HG] – host⊃guest concentration at equilibrium,
K_a^{HG} – binding constant of host⊃guest (HG) complex,
I^0 – background signal, I^{HD} – signal from host⊃dye (HD) complex, I^D – signal from free dye (D),

I_c – observable signal as a function of concentration

4 Determination of Binding Constants

4.1 Best Practice Guide for Thermodynamic GDA Procedure

1. Gather information on solubility of host and guest in solvent of interest.
2. Estimate binding constant of host-guest complex, e.g. by searching for related host-guest pairs on www.suprabank.org, www.supramolecular.org or in reviews.
3. Calculate which concentration of host and guest are needed to reach a sufficient (ideally ≥ 50%) degree of complexation of host. (A software package is available from the authors upon request and provided on GitHub: https://github.com/ASDSE/thermosimfit.) Excess of guest is permitted. If required guest concentration is within the solubility window, continue with step 5.
4. If required guest concentration is outside the solubility window, attempt to solubilize the guest in a solution of the host (sonication can help), followed by filtration/centrifugation and concentration determination of the host and guest concentration (e.g. by NMR, UV/Vis, HPLC etc., see section 7)
5. Simulate GDA by using Eq. S14 and adjust the indicator concentration and the host-guest concentration, while maintaining a sufficient degree of host-complexation (ideally ≥ 50%,[8] but also 10%-30% are processable). A software package is available from the authors upon request for simulations (provided also on GitHub: https://github.com/ASDSE/thermosimfit). Consider the solubility limit of the indicator dye. As a guideline, the dye should be chosen such that

$$\log K_a^{HG} + 2 \geq \log K_a^{HD} \geq \log K_a^{HG} - 1 \qquad \text{Eq. S15 (GDA)}$$

$$\log K_a^{HD} + 1 \geq \log K_a^{HG} \geq \log K_a^{HD} - 2 \qquad \text{Eq. S16 (GDA)}$$

   see the commencing section 3.2. Ideally, dyes that show stronger emission or distinct absorbance spectra upon host binding are chosen.
6. Simulate the host-dye binding curve in absence of guest for comparison. The GDA and host-dye curve should look sufficiently distinct (see Fig. 1a), if not, choose different concentrations or a different indicator dye.
7. Carry out the following experiments:
   i. GDA titration by addition of dye aliquots to the solution of the host-guest complex (**Fig. S1**, red dots and line). Wait after each injection until the system is equilibrated. Choose an excitation wavelength (e.g. red-onset of absorbance

band) such that the absorbance at this wavelength remains < 0.1 during the course of titration; otherwise inner filter effects will occur.

ii. Repeat the experiment with the same parameters, but in the absence of guest (**Fig. S1**, green dots and line). This host-dye binding curve should be distinct from the GDA curve. From the host-dye titration curve (use Eq. S5 for a DBA fitting, which is also implemented into the software package on request), the host-dye binding affinity and signal factors I^{HD} and I^{D} may be extracted if not known already.

iii. Titrate the dye into the blank solvent as a control using the same spectrometer settings. The resulting signal-concentration plot should look fairly linear (I^{D} can be derived as the slope of the linear fit), if not, complications such as dye-aggregation phenomena or inner filter effects[9] occur and a different indicator dye, excitation wavelength (if fluorescence based) or concentration range (dependent on guessed K_a^{HG}) should be utilized.

8. Fit the recorded GDA curves by using equations utilizing the predetermined K_a^{HD} and the exact concentrations as an input. (A software package is available from the authors upon request and provided on GitHub: https://github.com/ASDSE/thermosimfit.) The signal factors I^{HD} and I^{D} may be varied but their ratio should stay close to the expected value from the host-dye titration experiment. From the fitting, the host-guest binding affinity K_a^{HG} can be extracted.

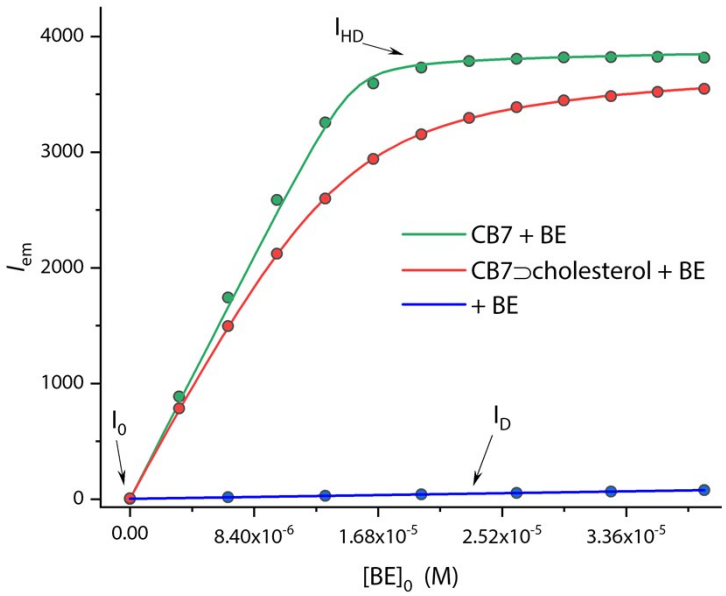

Fig. S1: Exemplified best practice procedure for obtaining accurate data with GDA featuring BE as indicator (λ_{exc} = 463 nm, λ_{em} = 570 nm) (blue dots and line display titration and fit into the bare solvent, respectively), CB7 as host (green dots and line display titration and fit of BE into a CB7 solution, respectively) and cholesterol as guest (red dots and line display titration and fit of BE into a CB7⊃cholesterol solution, respectively).

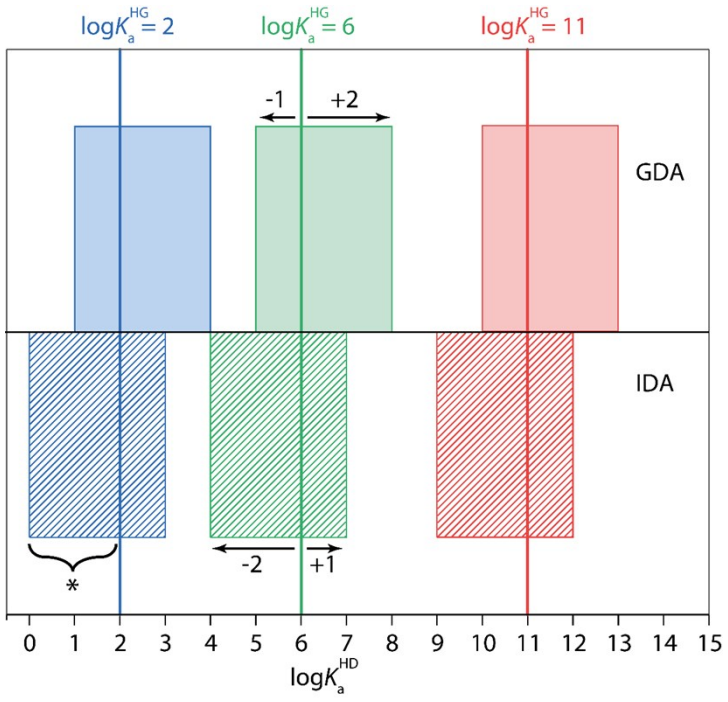

Fig. S2: Performance analysis of the competitive binding assays GDA and IDA. The coloured areas indicate the suitable affinity range of the indicator dye if a guest with an estimated affinity of logK_a = 2 (blue), 6 (green) or 11 (red) should be determined by GDA (solid bars) or IDA (striped bars). The asterisk indicates a region, where the high concentrations of H and D needed to obtain a suitable degree-of-complexation can cause photophysical artefacts (see best practice guide).

4.2 Derivation of Performance Window

In order to obtain meaningful binding constants from competitive-binding titration experiments, the acquired data must be reasonably fitable. In this context, the titration curve should be neither too linear nor too strongly bent. A simple method to predict and classify this curvature behavior is based on the slope of the first part of the titration and is presented here:

Firstly, a line is defined in the signal-intensity (with $I^{HD} = 1$, $I^{D} = 0$ and $I^{0} = 0$, which is in turn equal to the [HD] concentration at equilibrium) titration plot by connecting the starting point with the equilibrium point where $[competitor]_0 = [H]_0$, (1:1 host:guest binding is applied). Then the slope is obtained by a simple linear fit of the signal ([HD]) from 0 – $[H]_0$.

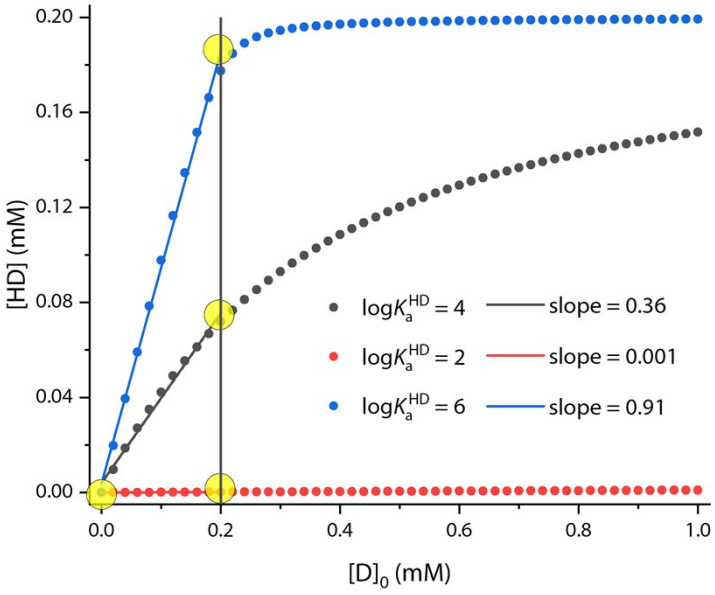

Fig. S3: GDA binding isotherm simulation and linear curve fitting to the corresponding equilibration point (0.2 mM) for dyes competing differently with a guest ($\log K_a^{HG} = 4$) for a host. The yellow spots indicate the end point (equilibration point where $[H]_0 = [D]_0$) and the starting point for the linear fitting.

In general, the slope is relatively flat or steep if a competitor binds weaker or stronger than the guest to the host, respectively. Our analysis showed that a slope below 0.1 is too low (~ 5° angle of intersection), whereas a slope above 0.9 is too high (~ 45° angle of intersection); titration curves that show such low or high slopes were found to result in poor affinity fits. Taking these boundaries into account, we systematically simulated the best performance window using Eq. S14 for various combinations of host-guest and host-indicator combinations.

For example, in GDA a guest with an affinity for the host of $\log K_a^{HG} = 4$ can be determined by competing indicators in the range from $\log K_a^{HD} = 3 - 6$, whereas $\log K_a^{HD} < 3$ yielded a simulated

titration curve that is too flat; if such a curve is used as a model curve for fitting of $\log K_a^{HG}$, then one observes that a range of $\log K_a^{HG}$ values can visually equally well fit the model data. This means such scenario is unsuitable in practice. Likewise, $\log K_a^{HD} > 6$ gave a too steep simulated binding curve that was unsuitable for back-fitting reliable of $\log K_a^{HG}$ values.

As a second example, the simulations showed that for a guest with $\log K_a^{HG} = 4$,indicators from $\log K_a^{HD} = 4 - 7$ should be used for GDA titrations. In general, we found that the $\log K_a^{HD}$ should lie again in the range of +2 ≥ $\log K_a^{HG}$ ≥ -1 for GDA, which is Eq. S17. These simulations explain well the experimental findings that a very strong binding between cadaverine and CB7 (logK_a = 8.37) (performance simulations see Fig. S6) could not be accurately determined by a GDA utilizing BE (logK_a = 7.23) (CB7⊃cadaverine logK_a = 7.98). Analysis of the performance chart suggests the usage of a stronger indicator such as MDAP (logK_a = 9.43), which indeed leads to more accurate value of (logK_a = 8.64) being comparable to the one determined by an IDA.

A similar performance chart can be created for IDA, which is read differently. Here the $\log K_a^{HD}$ of the host:indicator is fixed and one looks up the guest that can accurately be determined by the displacement of the indicator (Fig. S7). This simulation rationalizes why the binding of *n*-butanol to β-CD (logK_a = 2.00) cannot be accurately determined by an IDA (Fig. S26) using TNS (logK_a = 3.83), the guest affinity lies simply outside the performance window for this indicator. The use of the corresponding GDA performance chart for this indicator (Fig. S4) predicts reasonable data for the titration experiment, which was experimentally validated (Fig. S27). Analogously, for IDA we derived the following recommended performance window

$$\log K_a^{HD} + 2 \geq \log K_a^{HG} \geq \log K_a^{HD} - 1 \qquad \text{Eq. S18 (IDA)}$$

$$\log K_a^{HG} + 1 \geq \log K_a^{HD} \geq \log K_a^{HG} - 2 \qquad \text{Eq. S19 (IDA)}$$

4.2.1 Details for Performance Chart Simulations

For a GDA performance chart, the equation Eq. S14 (I_0 = 0; I_{HD} = 1, I_D = 0) was fed with the following parameters $\log K_a^{HG}$ (e.g. 4), $[H]_0 = [G]_0 = 2*K_d^{HG}$ (e.g. 200 µM), $[D]_0 = 0 – 5*K_d^{HG}$ (e.g. 0 – 500 µM), while the $\log K_a^{HD}$ (e.g. 0 – 10)was varied for each point of slope in the resulting graph. The slope was determined by a linear fit from 0 – $[H]_0$.

For a IDA performance chart, the equation Eq. S14 (I_0 = 0; I_{HD} = 1, I_D = 0) was fed with the following parameters: $\log K_a^{HD}$ (e.g. 4), $[H]_0 = [D]_0 = 2*K_d^{HD}$ (e.g. 200 µM), $[G]_0 = 0 – 5*K_d^{HD}$ (e.g. 0 – 500 µM), while the $\log K_a^{HG}$ (e.g. 0 – 10) was varied for each point of slope in the resulting graph. The slope was determined by a linear fit from 0 – $[H]_0$ on a pre-normalized (compensation for the initial 50% degree of complexation of the host) so that $[H]_0$ is the maximum of the function output (dependent variable) dataset.

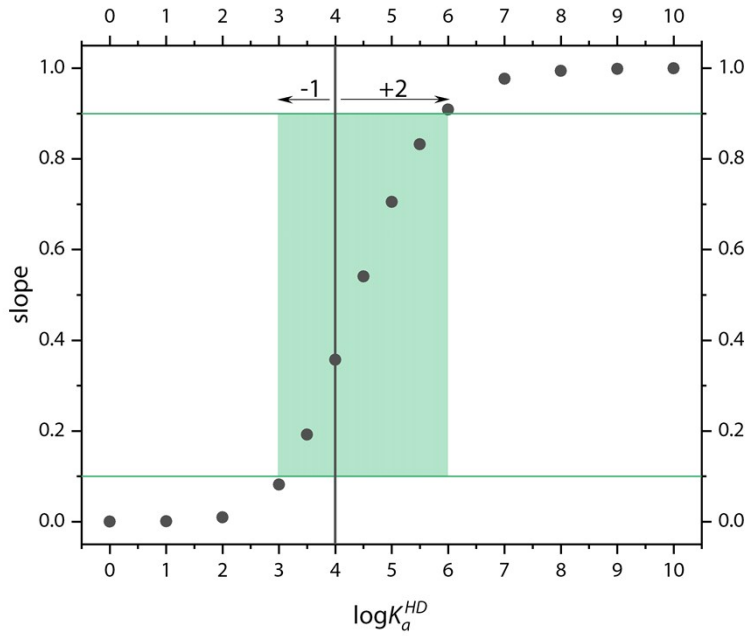

Fig. S4: Performance chart for a GDA to accurately determine the binding constant of a host:guest pair featuring a $\log K_a^{HG} = 4$ (indicated by the black vertical line). The green window indicates the range of best performing indicator which is limited by the upper (0.9) and lower (0.1) slope boundaries.

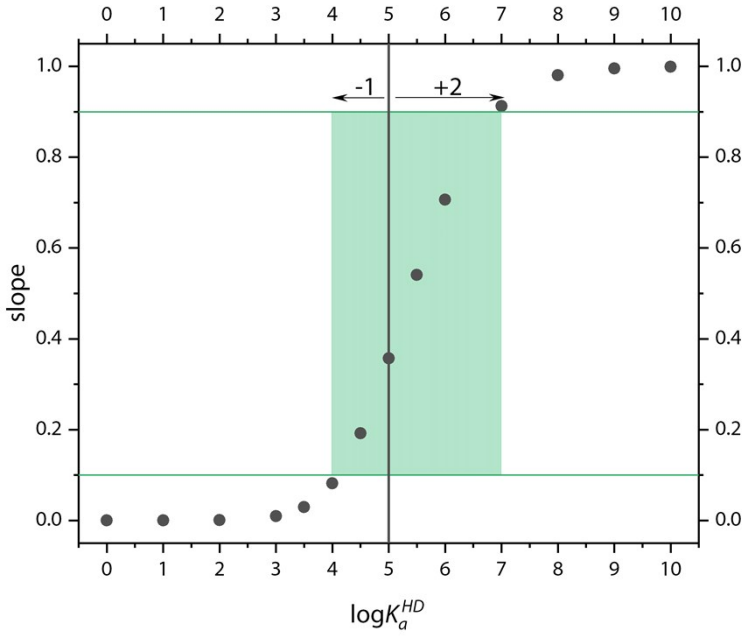

Fig. S5: Performance chart for a GDA to accurately determine the binding constant of a host:guest pair featuring a $\log K_a^{HG} = 5$ (indicated by the black vertical line). The green window indicates the range of best performing indicator which is limited by the upper (0.9) and lower (0.1) slope boundaries.

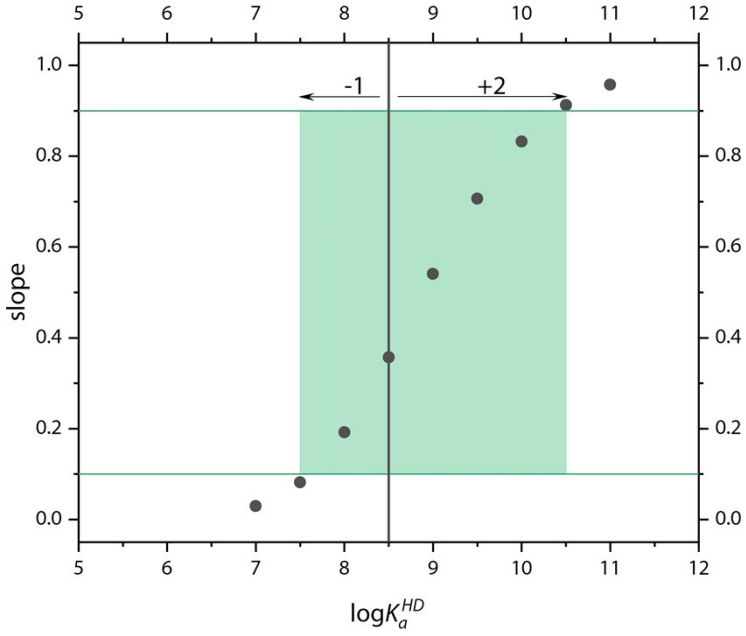

Fig. S6: Performance chart for a GDA to accurately determine the binding constant of a host:guest pair featuring a $\log K_a^{HG} = 8.5$ (indicated by the black vertical line). The green window indicates the range of best performing indicator which is limited by the upper (0.9) and lower (0.1) slope boundaries.

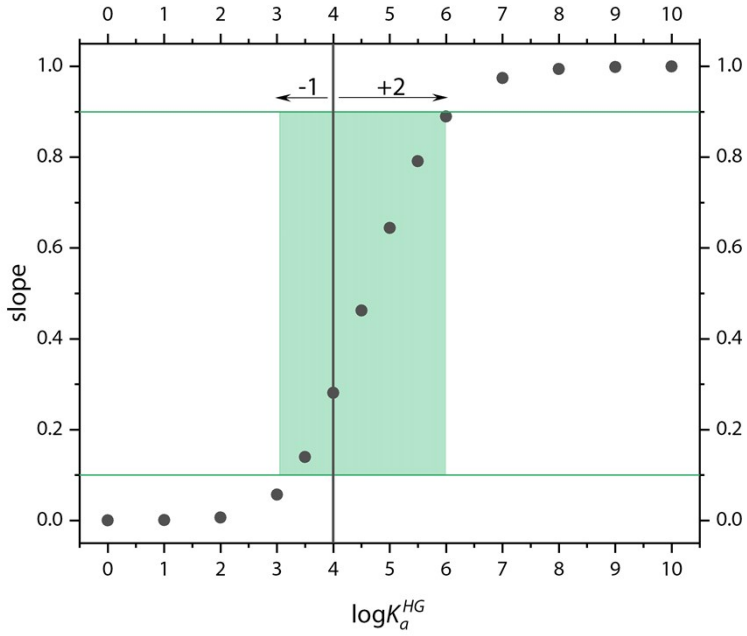

Fig. S7: Performance chart for a IDA to accurately determine the binding constant of a host:guest pair featuring a $\log K_{\mathrm{a}}^{\mathrm{HD}} = 4$ (indicated by the black vertical line). The green window indicates the range of best performing indicator which is limited by the upper (0.9) and lower (0.1) slope boundaries.

4.3 Binding Affinities

Table S3: Binding affinities for analyzed guests towards different hosts.

guest	host	dye	**logK_a^{HG} (M^{-1})**	method
ethanol (5.27 mM)	CB7 (56 µM)	TNS (0 – 567 µM)	2.49 ± 0.01	GDA
ethanol (7.05 mM)	β-CD (100 µM)	TNS(0 – 691 µM)	1.93 ± 0.01	GDA
iso-propanol (1.05 mM)	β-CD (103 µM)	TNS(0 – 598 µM)	2.27 ± 0.02	GDA
n-butanol (292 µM)	CB7 (50 µM)	TNS (0 – 568 µM)	4.89 ± 0.04	GDA
n-butanol (0 – 654 µM)	CB7 (21 µM)	TNS (0 – 79 µM)	4.69 ± 0.02	IDA
n-butanol (884 µM)	β-CD (100 µM)	TNS (0 – 594 µM)	2.00 ± 0.04	GDA
n-butanol (0 – 6 mM)	β-CD (60 µM)	TNS (703 µM)	2.17 [a]	IDA
t-butanol (932 µM)	β-CD (100 µM)	TNS (0 – 598 µM)	2.26 ± 0.08	GDA
1-adamantanol (100 µM)	β-CD (33 µM)	TNS (0 – 598 µM)	4.75 [a]	GDA
1-adamantanol (0 – 366 µM)	β-CD (100 µM)	TNS (100 µM)	5.01 ± 0.08	IDA
cadaverine (4.3 µM)	CB7 (2 µM)	BE (0 - 26 µM)	7.98 [a]	GDA
cadaverine (0 - 29 µM)	CB7 (1.3 µM)	BE (23 µM)	8.37 ± 0.05	IDA
cadaverine (2 µM)	CB7 (1.2 µM)	MDAP (0 – 3.6 µM)	8.64 ± 0.03	GDA
methyl viologen (4 µM)	CB7 (3 µM)	MDAP(0 – 7 µM)	8.78 ± 0.01	GDA
methyl viologen (0 – 9 µM)	CB7 (4.3 µM)	BE (6 µM)	8.84 ± 0.04	IDA
cholesterol[a] (25 µM)	CB7 (15 µM)	BE (0 – 39 µM)	5.91 ± 0.04	GDA
estradiol (13 µM)	CB7 (16.5 µM)	BE (0 – 45.6 µM)	6.25 ± 0.11	GDA
progesterone (36 µM)	CB7 (93 µM)	TNS (0 – 713 µM)	4.77 ± 0.08	GDA
progesterone	CB7	BE	–	GDA
nortestosterone (0.7 µM)	CB8 (0.6 µM)	BE (0 – 13 µM)	8.19 ± 0.09	GDA
phenylbutazone [b] (21 µM)	HSA (10 µM)	warfarin (0 – 32 µM)	5.83 ± 0.04	GDA
warfarin [c] (0 – 32 µM)	HSA (10 µM)		5.15 ± 0.04	DBA
TNS (27 µM)	CB7 (0 – 140 µM)		4.53 ± 0.04	DBA
TNS [d] (826 µM)	β-CD (0 – 840 µM)		3.38 ± 0.02	DBA
BE (0.8 µM)	CB7 (0 – 2.7 µM)		7.23 ± 0.10	DBA
MDAP (0 – 9.3 µM)	CB7 (5 µM)	BE (6 µM)	9.43 ± 0.02	IDA

[a] Due to a mismatch of the binding affinities (Eq. S20 and Eq. S21) this value is considered to be not as accurate as the one determined by the alternative competitive binding assay or a modification of the reporter pair setup. Literature References: [b] logK_a = 5.41, *via* Scatchard plot.[10] [c] logK_a = 5.44 *via* Scatchard plot.[10] [d] logK_a = 3.04.[11]

4.3.1 CB7⊃BE

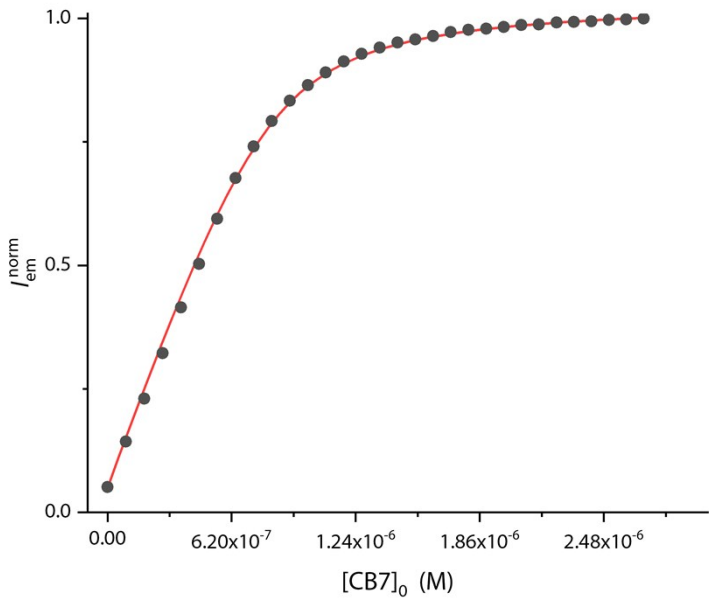

Fig. S8: Representative DBA binding isotherm determined by fluorescence intensity variations (λ_{exc} = 421 nm, λ_{em} = 542 nm) of BE (0.8 µM) and CB7 (0 – 2.7 µM) in water at 25°C. Acquired data is depicted as gray dots and fitted data as red line.

4.3.2 CB7⊃estradiol

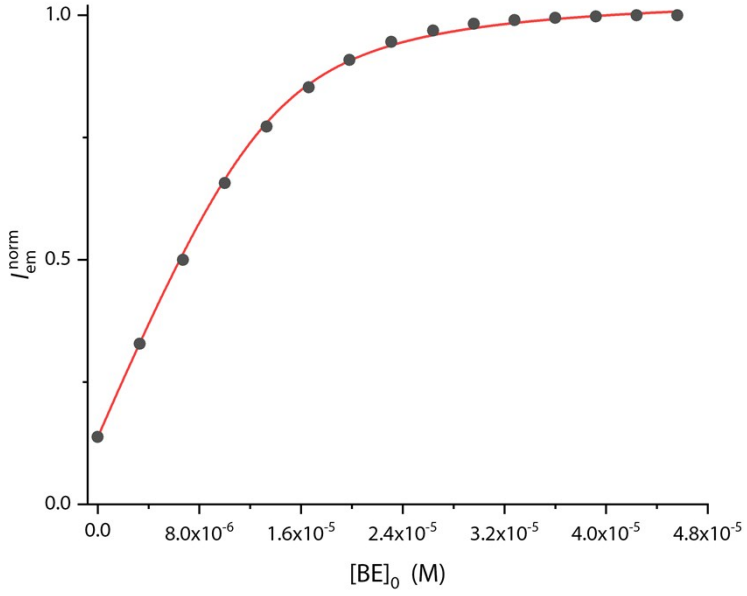

Fig. S9: Representative GDA binding isotherm determined by fluorescence intensity variations (λ_{exc} = 421 nm, λ_{em} = 542 nm) of BE (0 – 45.6 µM) and CB7 (16.5 µM) and estradiol (13 µM) in water at 25°C. Acquired data is depicted as gray dots and fitted data as red line.

4.3.3 CB7⊃cholesterol

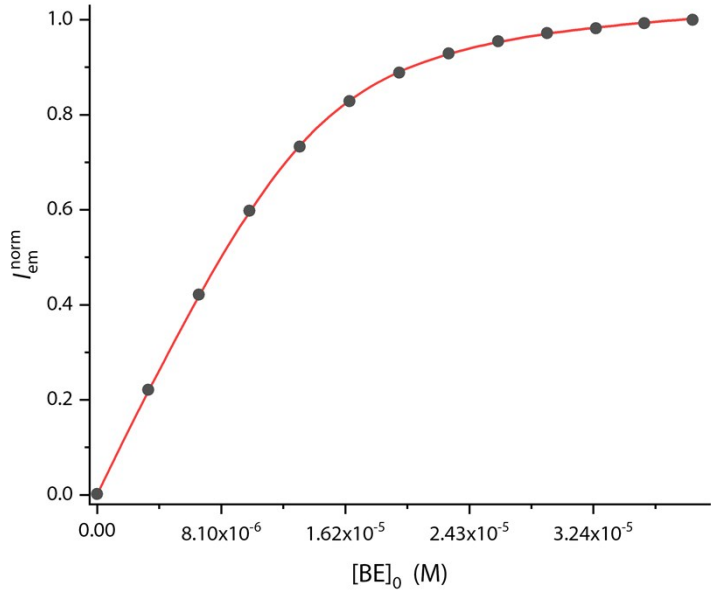

Fig. S10: Representative GDA binding isotherm determined by fluorescence intensity variations (λ_{exc} = 463 nm, λ_{em} = 570 nm) of BE (0 – 39 μM), CB7 (15 μM) and cholesterol (25 μM) in water/ethanol (95.5/0.5, v/v) at 25°C. Acquired data is depicted as gray dots and fitted data as red line.

4.3.4 CB7⊃TNS

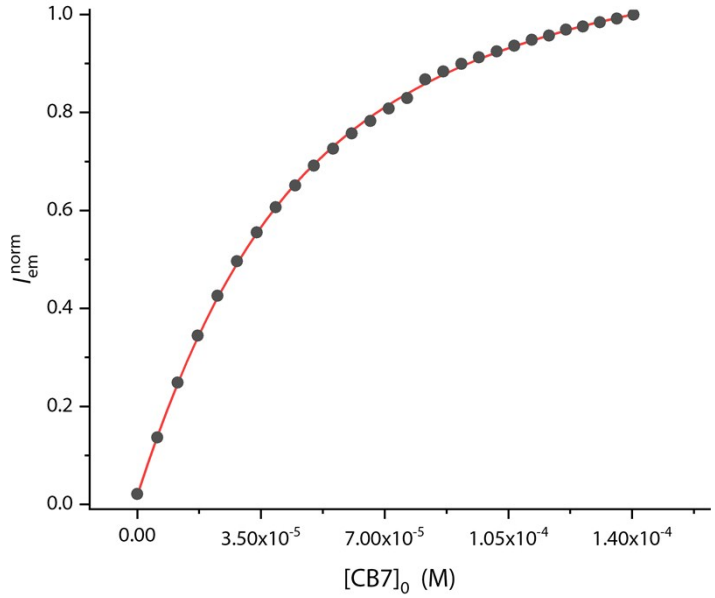

Fig. S11: Representative DBA binding isotherm determined by fluorescence intensity variations (λ_{exc} = 405 nm, λ_{em} = 550 nm) of TNS (27 μM) and CB7 (0 – 140 μM) in water at 25°C. Acquired data is depicted as gray dots and fitted data as red line.

4.3.5 CB7⊃progesterone

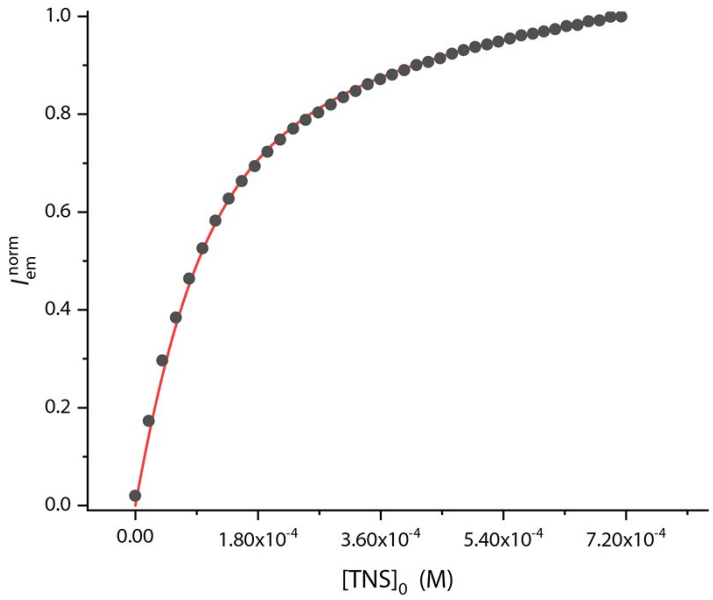

Fig. S12: Representative GDA binding isotherm determined by fluorescence intensity variations (λ_{exc} = 405 nm, λ_{em} = 550 nm) of TNS (0 – 713 µM), CB7 (93 µM) and progesterone (36 µM) in water at 25°C. Acquired data is depicted as gray dots and fitted data as red line.

4.3.6 CB7⊃*n*-butanol

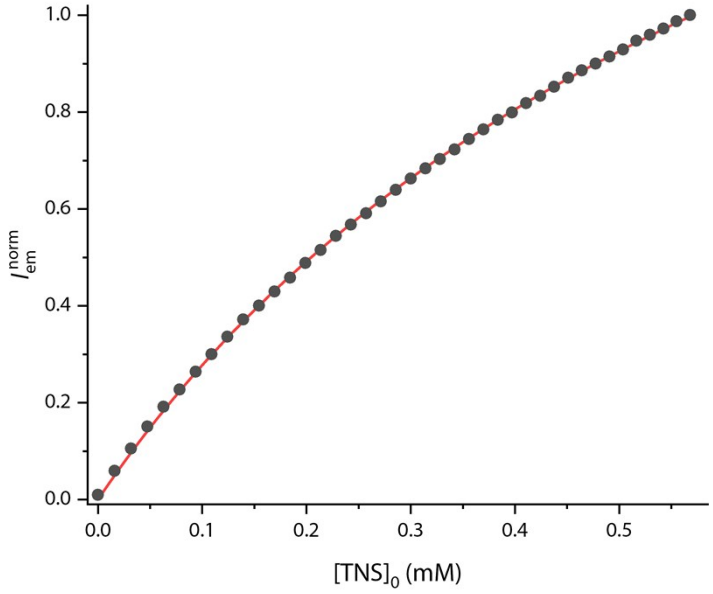

Fig. S13: Representative GDA binding isotherm determined by fluorescence intensity variations (λ_{exc} = 405 nm, λ_{em} = 550 nm) of TNS (0 – 568 µM) and CB7 (50 µM) and *n*-butanol (292 µM) in water at 25°C. Acquired data is depicted as gray dots and fitted data as red line.

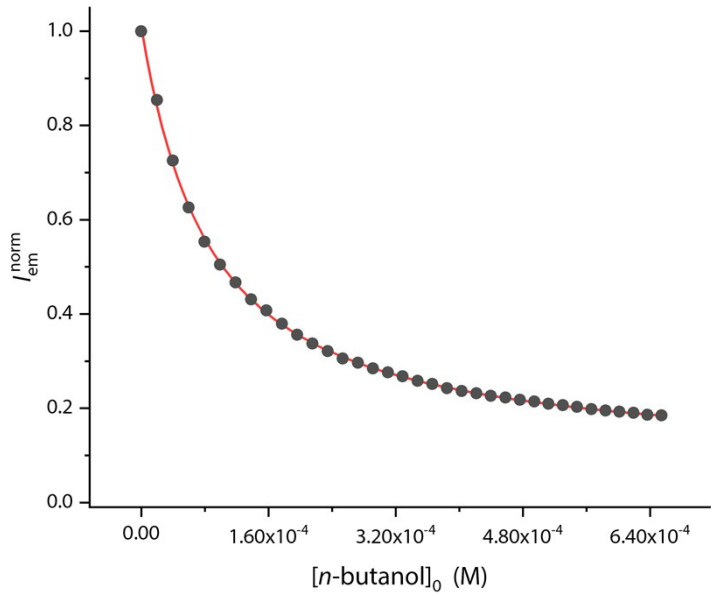

Fig. S14: Representative IDA binding isotherm determined by fluorescence intensity variations (λ_{exc} = 405 nm, λ_{em} = 550 nm) of TNS (79 µM), CB7 (21 µM) and *n*-butanol (0 – 654 µM) in water at 25°C. Acquired data is depicted as gray dots and fitted data as red line.

4.3.7 CB7⊃ethanol

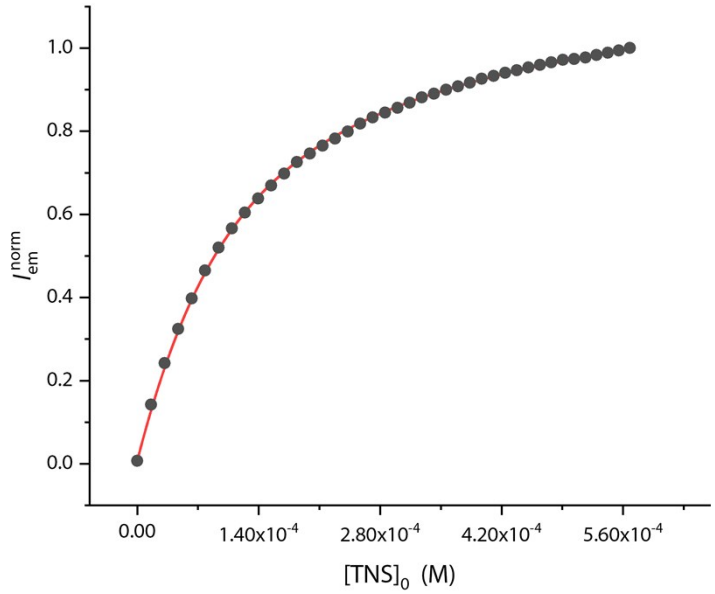

Fig. S15: Representative GDA binding isotherm determined by fluorescence intensity variations (λ_{exc} = 405 nm, λ_{em} = 550 nm) of TNS (0 – 567 µM), CB7 (56 µM) and ethanol (5.27 mM) in water at 25°C. Acquired data is depicted as gray dots and fitted data as red line.

4.3.8 CB7⊃MDAP

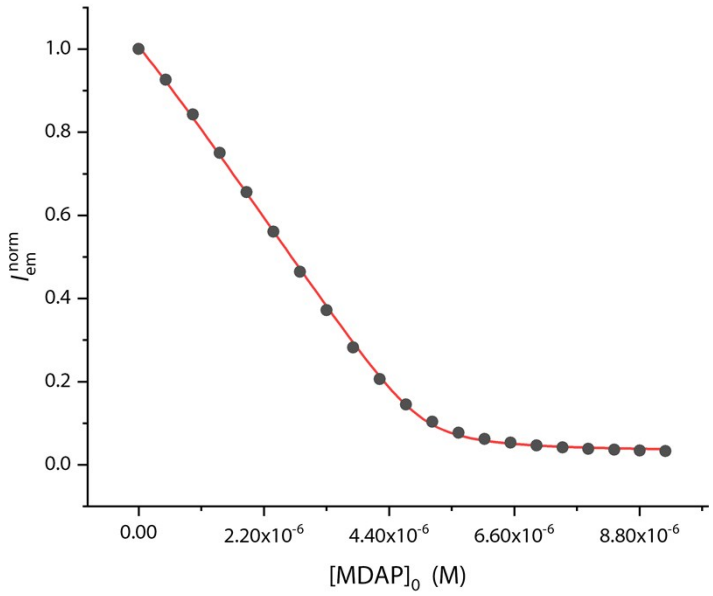

Fig. S16: Representative IDA binding isotherm determined by fluorescence intensity variations (λ_{exc} = 421 nm, λ_{em} = 542 nm) of BE (6 µM), CB7 (5 µM) and MDAP (0 – 9.3 µM) in water at 25°C. Acquired data is depicted as gray dots and fitted data as red line.

4.3.9 CB7⊃cadaverine

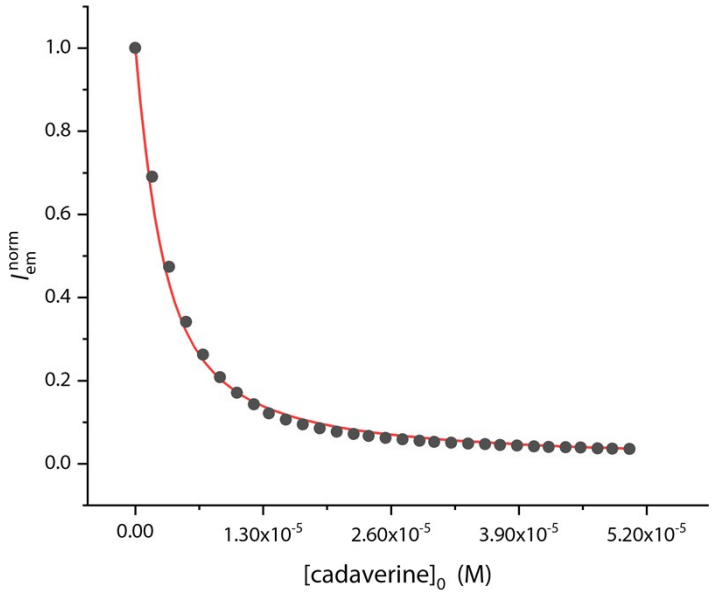

Fig. S17: Representative IDA binding isotherm determined by fluorescence intensity variations (λ_{exc} = 463 nm, λ_{em} = 570 nm) of BE (23 µM), CB7 (1.3 µM) and cadaverine (0 – 29 µM) in water at 25°C. Acquired data is depicted as gray dots and fitted data as red line.

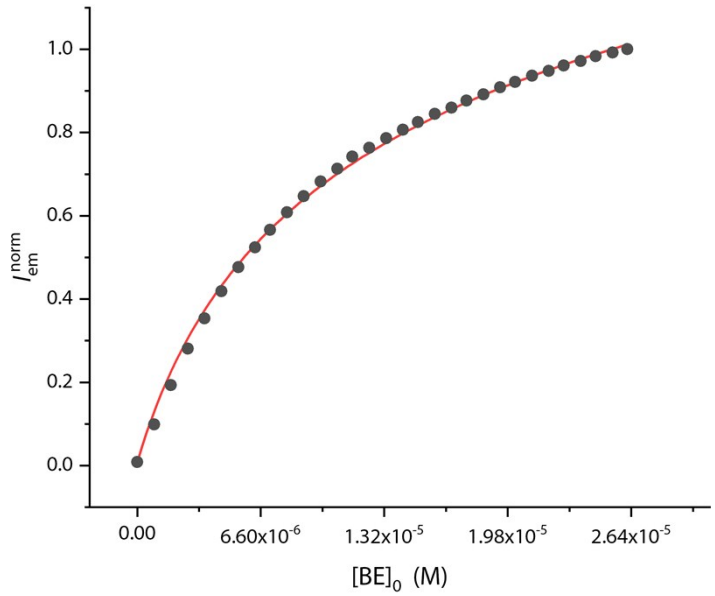

Fig. S18: Representative GDA binding isotherm determined by fluorescence intensity variations (λ_{exc} = 421 nm, λ_{em} = 542 nm) of BE (0 – 26 µM), CB7 (2 µM) and cadaverine (4.3 µM) in water at 25°C. Acquired data is depicted as gray dots and fitted data as red line. Note: The binding affinity of the guest is considerably high in comparison to the dye towards the host, thus, in order to obtain a more accurate K_a value, a stronger binding indicator was utilized (see Fig. S19).

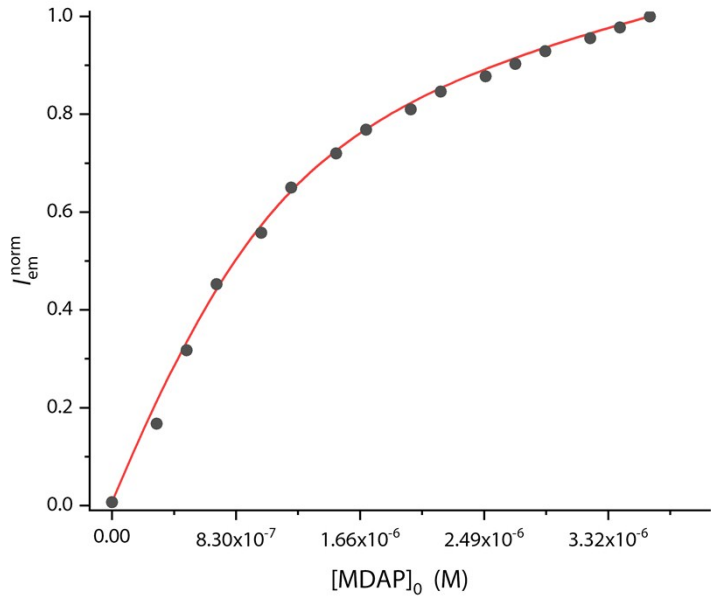

Fig. S19: Representative GDA binding isotherm determined by fluorescence intensity variations (λ_{exc} = 343 nm, λ_{em} = 454 nm) of MDAP (0 – 3.6 µM), CB7 (1.2 µM) and cadaverine (2 µM) in water at 25°C. Acquired data is depicted as gray dots and fitted data as red line.

4.3.10 CB7⊃MV

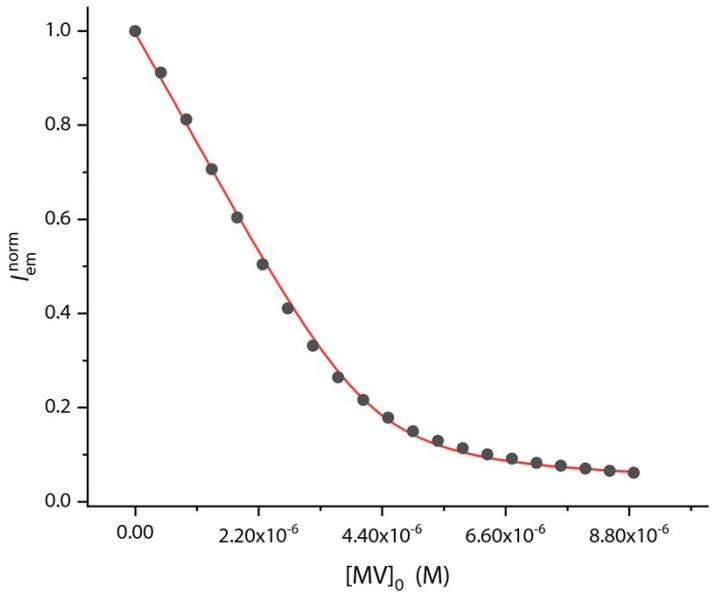

Fig. S20: Representative IDA binding isotherm determined by fluorescence intensity variations (λ_{exc} = 421 nm, λ_{em} = 542 nm) of BE (6 μM), CB7 (4.3 μM) and methyl viologen (0 – 9 μM) in water at 25°C. Acquired data is depicted as gray dots and fitted data as red line.

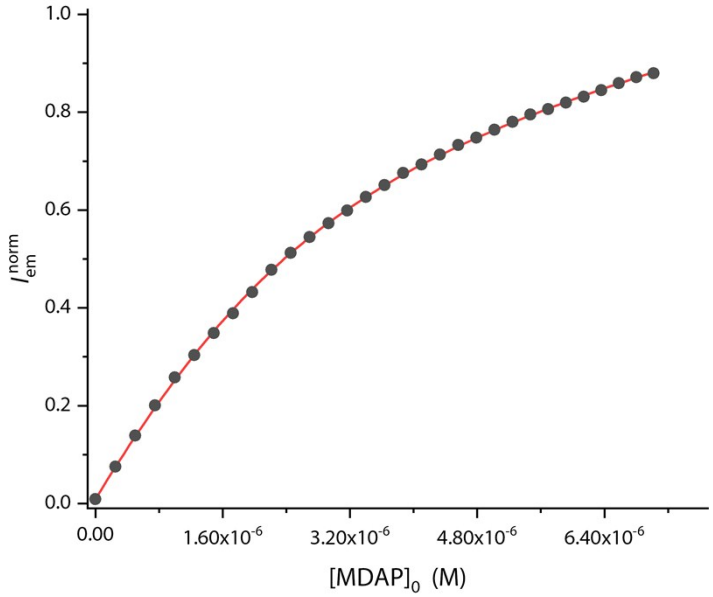

Fig. S21: Representative GDA binding isotherm determined by fluorescence intensity variations (λ_{exc} = 343 nm, λ_{em} = 454 nm) of MDAP (0 – 7 μM), CB7 (3 μM) and methyl viologen (4 μM) in water at 25°C. Acquired data is depicted as gray dots and fitted data as red line.

4.3.11 CB8⊃nortestosterone

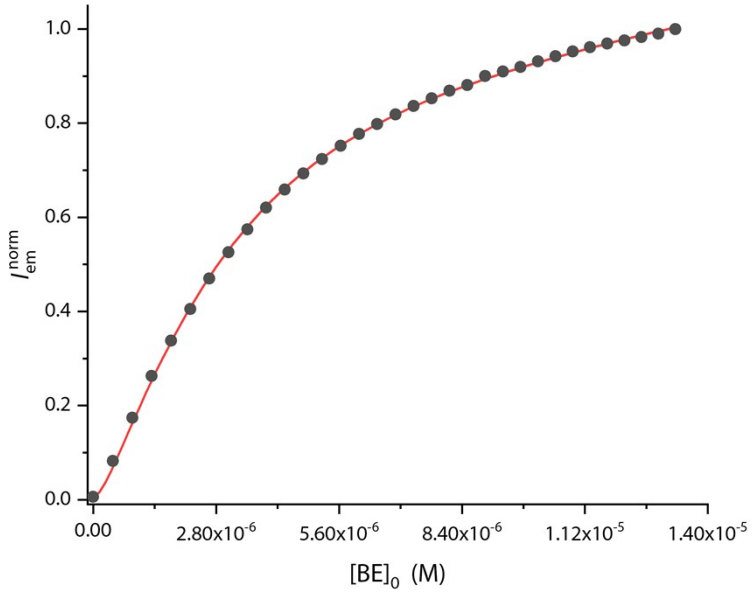

Fig. S22: Representative GDA binding isotherm determined by fluorescence intensity variations (λ_{exc} = 421 nm, λ_{em} = 542 nm) of BE (0 – 13 μM), CB8 (0.6 μM) and nortestosterone (0.7 μM) in water at 25°C. Acquired data is depicted as gray dots and fitted data as red line.

4.3.12 β-CD⊃TNS

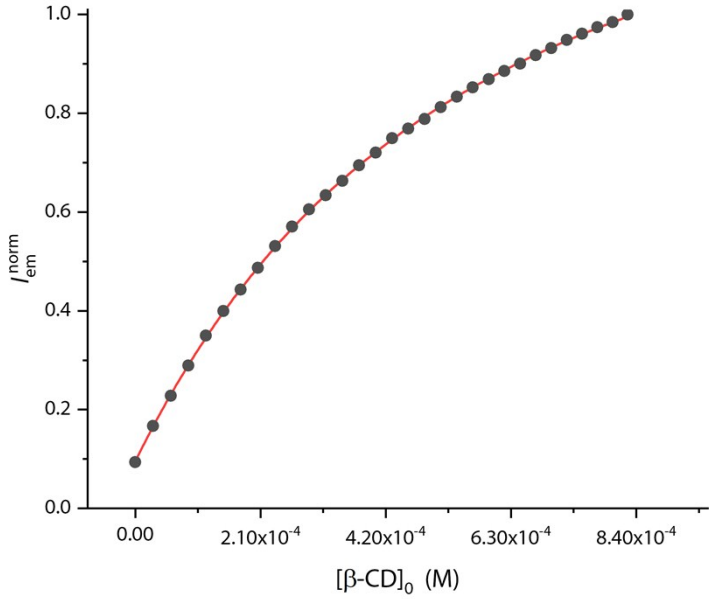

Fig. S23: Representative DBA binding isotherm determined by fluorescence intensity variations (λ_{exc} = 405 nm, λ_{em} = 550 nm) of TNS (826 μM) and β-CD (0 – 840 μM) in water at 25°C. Acquired data is depicted as gray dots and fitted data as red line.

4.3.13 β-CD⊃ethanol

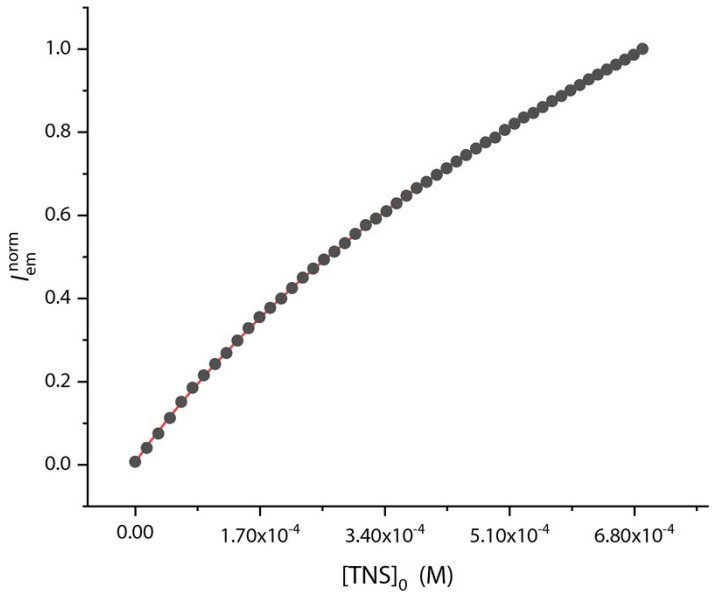

Fig. S24: Representative GDA binding isotherm determined by fluorescence intensity variations (λ_{exc} = 405 nm, λ_{em} = 550 nm) of TNS (0 – 691 µM), β-CD (100 µM) and ethanol (7.05 mM) in water at 25°C. Acquired data is depicted as gray dots and fitted data as red line.

4.3.14 β-CD⊃*iso*-propanol

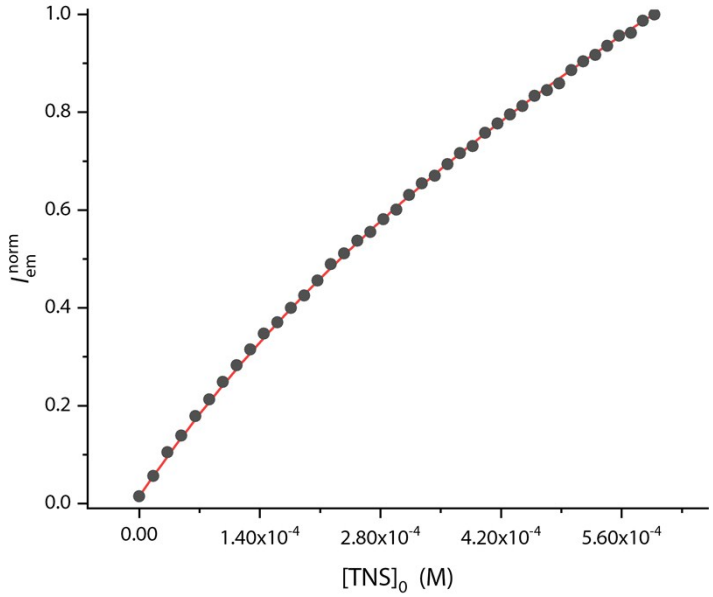

Fig. S25: Representative GDA binding isotherm determined by fluorescence intensity variations (λ_{exc} = 405 nm, λ_{em} = 550 nm) of TNS (0 – 598 µM), β-CD (103 µM) and *iso*-propanol (1.05 mM) in water at 25°C. Acquired data is depicted as gray dots and fitted data as red line.

4.3.15 β-CD⊃*n*-butanol

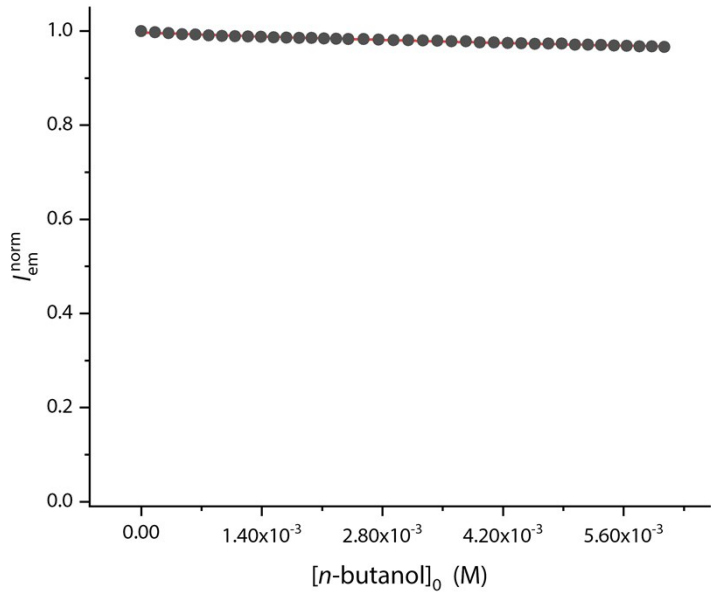

Fig. S26: Representative IDA binding isotherm determined by fluorescence intensity variations (λ_{exc} = 405 nm, λ_{em} = 550 nm) of TNS (703 µM) and β-CD (60 µM) and *n*-butanol (0 – 6 mM) in water at 25°C. Acquired data is depicted as gray dots and fitted data as red line. Note: Due to a mismatch of the binding affinities this value is considered to be not as accurate as the one determined by the alternative competitive binding assay.

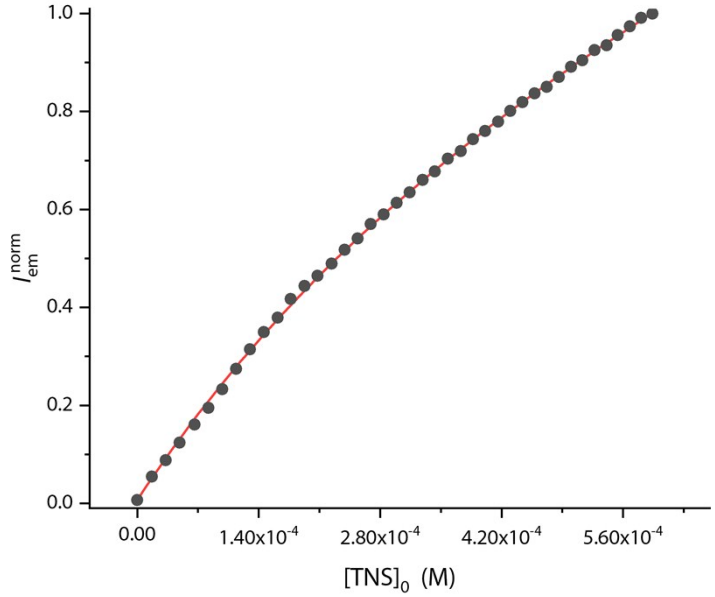

Fig. S27: Representative GDA binding isotherm determined by fluorescence intensity variations (λ_{exc} = 405 nm, λ_{em} = 550 nm) of TNS (0 – 594 µM) and β-CD (100 µM) and *n*-butanol (884 µM) in water at 25°C. Acquired data is depicted as gray dots and fitted data as red line.

4.3.16 β-CD⊃*t*-butanol

Fig. S28: Representative GDA binding isotherm determined by fluorescence intensity variations (λ_{exc} = 405 nm, λ_{em} = 550 nm) of TNS (0 – 598 µM) and β-CD (100 µM) and *t*-butanol (932 µM) in water at 25°C. Acquired data is depicted as gray dots and fitted data as red line.

4.3.17 β-CD⊃1-adamantanol

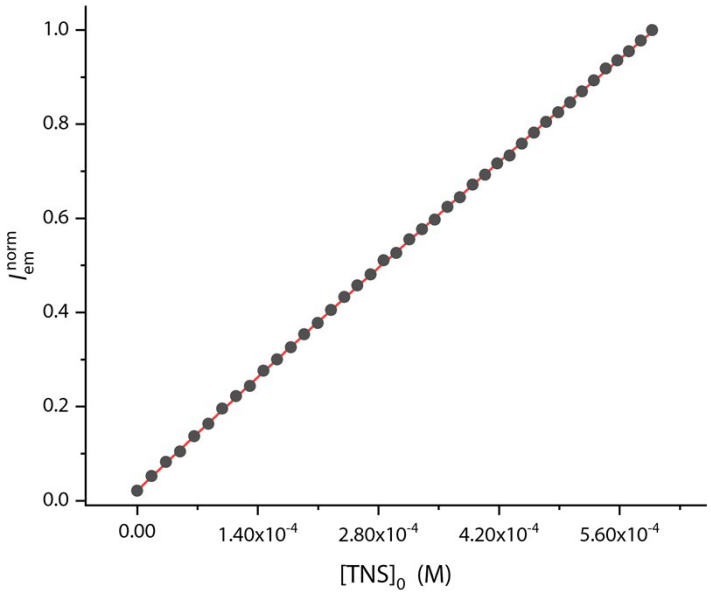

Fig. S29: Representative GDA binding isotherm determined by fluorescence intensity variations (λ_{exc} = 405 nm, λ_{em} = 550 nm) of TNS (0 – 598 µM) and β-CD (33 µM) and 1-adamantanol (100 µM) in water at 25°C. Acquired data is depicted as gray dots and fitted data as red line. Note: Due to a mismatch of the binding affinities this value is considered to be not as accurate as the one determined by the alternative competitive binding assay.

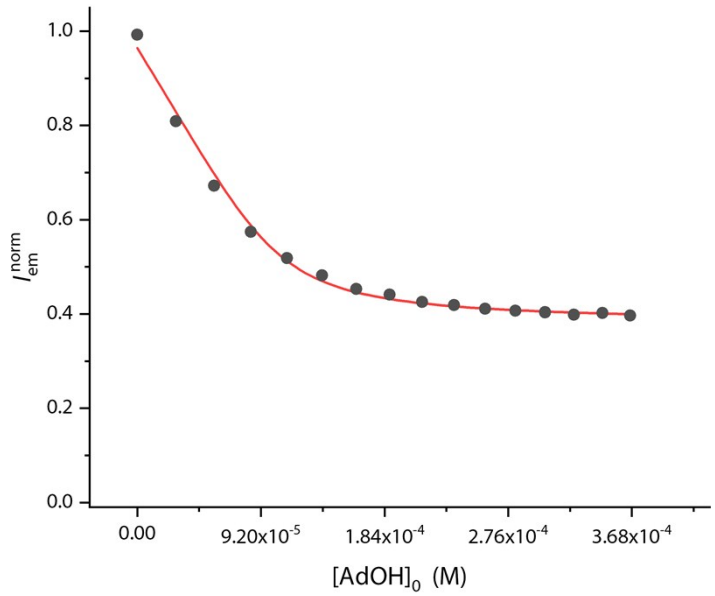

Fig. S30: Representative IDA binding isotherm determined by fluorescence intensity variations (λ_{exc} = 405 nm, λ_{em} = 550 nm) of TNS (100 µM) and β-CD (100 µM) and 1-adamantanol (0 – 366 µM) in water at 25°C. Acquired data is depicted as gray dots and fitted data as red line.

4.3.18 HSA⊃warfarin

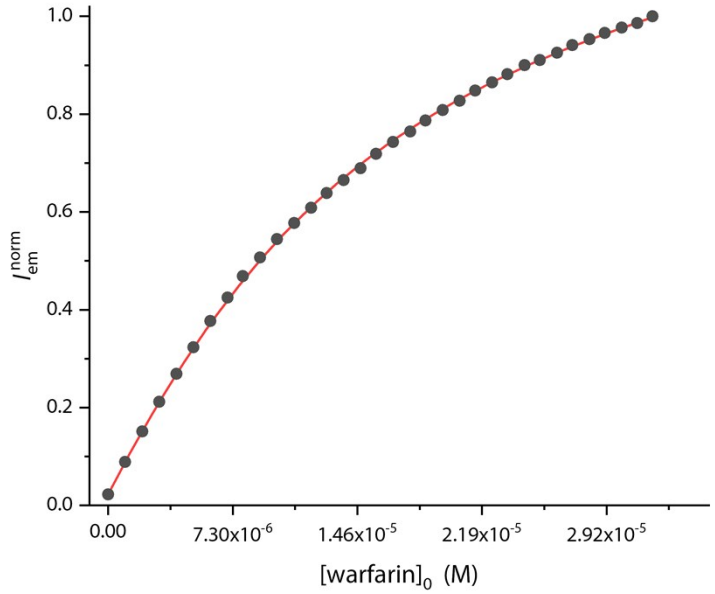

Fig. S31: Representative DBA binding isotherm determined by fluorescence intensity variations (λ_{exc} = 335 nm, λ_{em} = 410 nm) of warfarin (0 – 32 µM) and HSA (10 µM) in PBS at 25°C. Acquired data is depicted as gray dots and fitted data as red line.

4.3.19 HSA⊃phenylbutazone

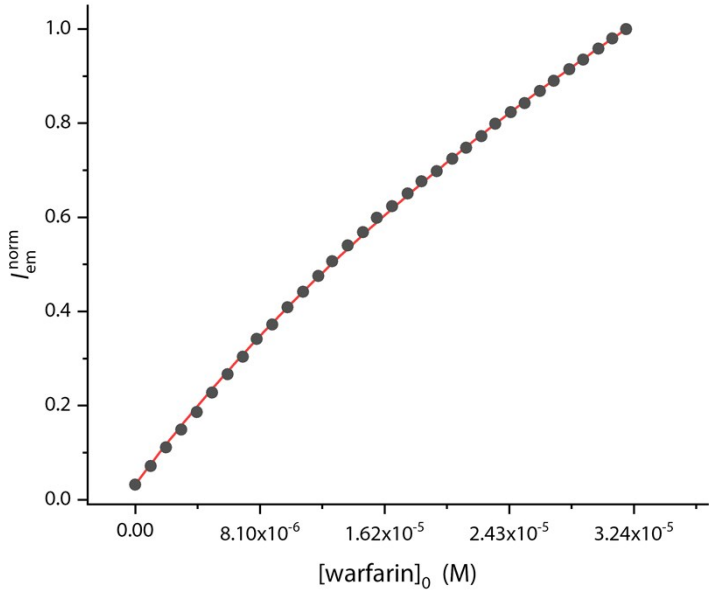

Fig. S32: Representative GDA binding isotherm determined by fluorescence intensity variations (λ_{exc} = 335 nm, λ_{em} = 410 nm) of warfarin (0 – 32 µM), PBZ (21 µM) and HSA (10 µM) in PBS at 25°C. Acquired data is depicted as gray dots and fitted data as red line.

5 Determination of Concentrations of Host-Guest Complexes by NMR

The concentration determination of all insoluble guest molecules where carried out via ^{1}HNMR measurements in D_2O with a dimethyl sulfone as a common standard.

For the measurement, the host-guest stock solution was prepared in D_2O and sonicated for 10 min. Afterwards, 0.25 ml of the solution were mixed with 0.25 ml of a dimethyl sulfone stock solution of which the concentration was known. The NMR measurement was then carried out on a Bruker Avance 500 spectrometer.

The obtained spectra were phase and baseline corrected and the calibrated to the solvent peak of D_2O. The signal of dimethyl sulfone at 3.08 ppm was used as a reference with a total integral of 6 protons. The integration of certain host and guest signals lead to the determination of the concentration of each compound.

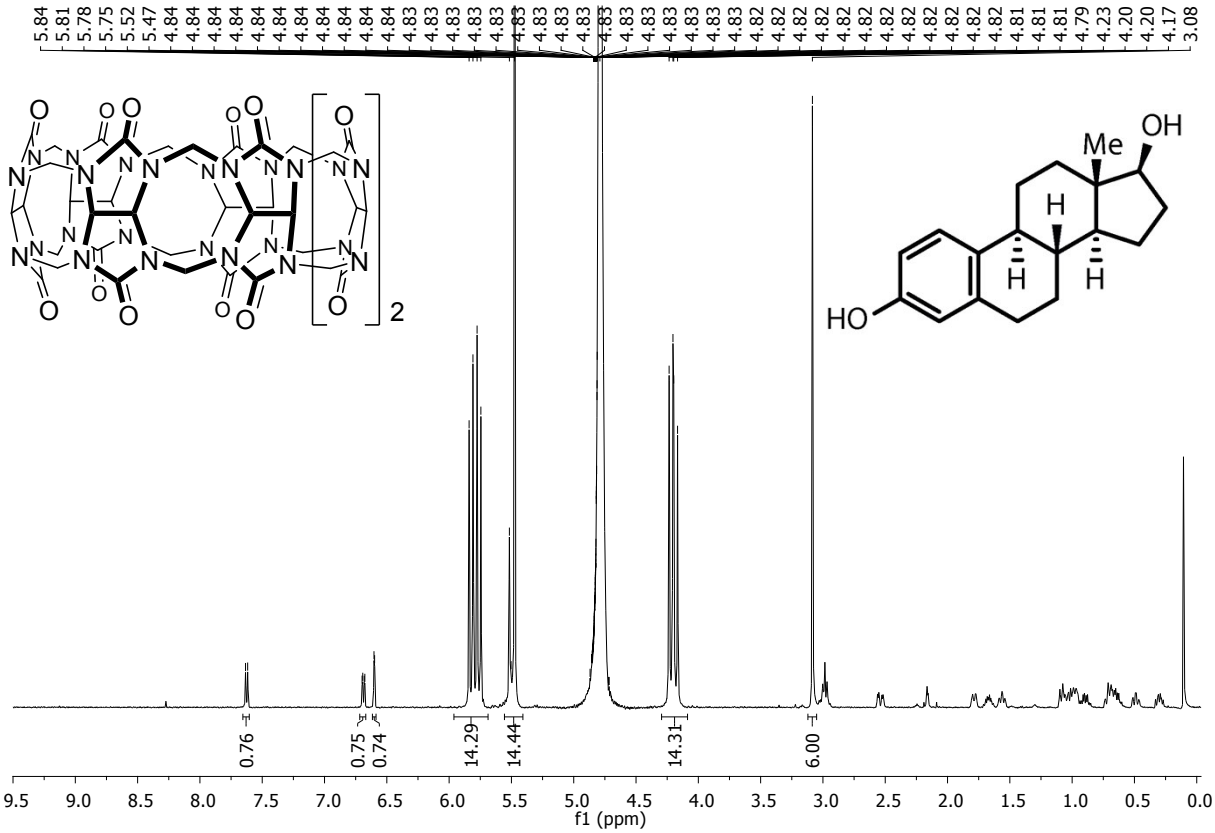

Fig. S33: ^{1}H-NMR (500 MHz, D_2O) spectrum of the CB7/estradiol complex. All signals in the region of 0.20 to 2.60ppm and 6.60 to 7.63ppm can be referred to estradiol. For the concentration determination of estradiol only the signal from 6.60 to 7.63 ppm were integrated and used. The signals in in the region 4.17 to 4.23ppm and 5.47 to 5.84ppm can be referred to CB7, they were all used for the concentration determination of CB7. The signal at 3.08ppm can be referred to dimethyl sulfone, which was used as a proton reference for the concentration determination of all compounds.

Table S4: Calculation of the concentration of CB7 (top) and estradiol (bottom) *via* the received Integrals from **Fig. S33**.

species	integral	protons	norm. integral	divisor	conc. [mM]
DMS	6.00	6.0	1.00000		1.00000
CB7-1	14.31	14.0	1.02214	0.97834	1.02214
CB7-2	14.44	14.0	1.03143	0.96953	1.03143
CB7-3	14.29	14.0	1.02071	0.97971	1.02071
CB7-Mean					1.02476
CB7-StDev					0.00582

species	integral	protons	norm. integral	divisor	conc. [mM]
DMS	6.00	6.00	1.00000		1.00000
estradiol	0.74	1.00	0.74000	1.35135	0.74000
estradiol	0.75	1.00	0.75000	1.35135	0.74000
estradiol	0.76	1.00	0.76000	1.31579	0.76000
estradiol-Mean					0.74667
estradiol-StDev					0.00943

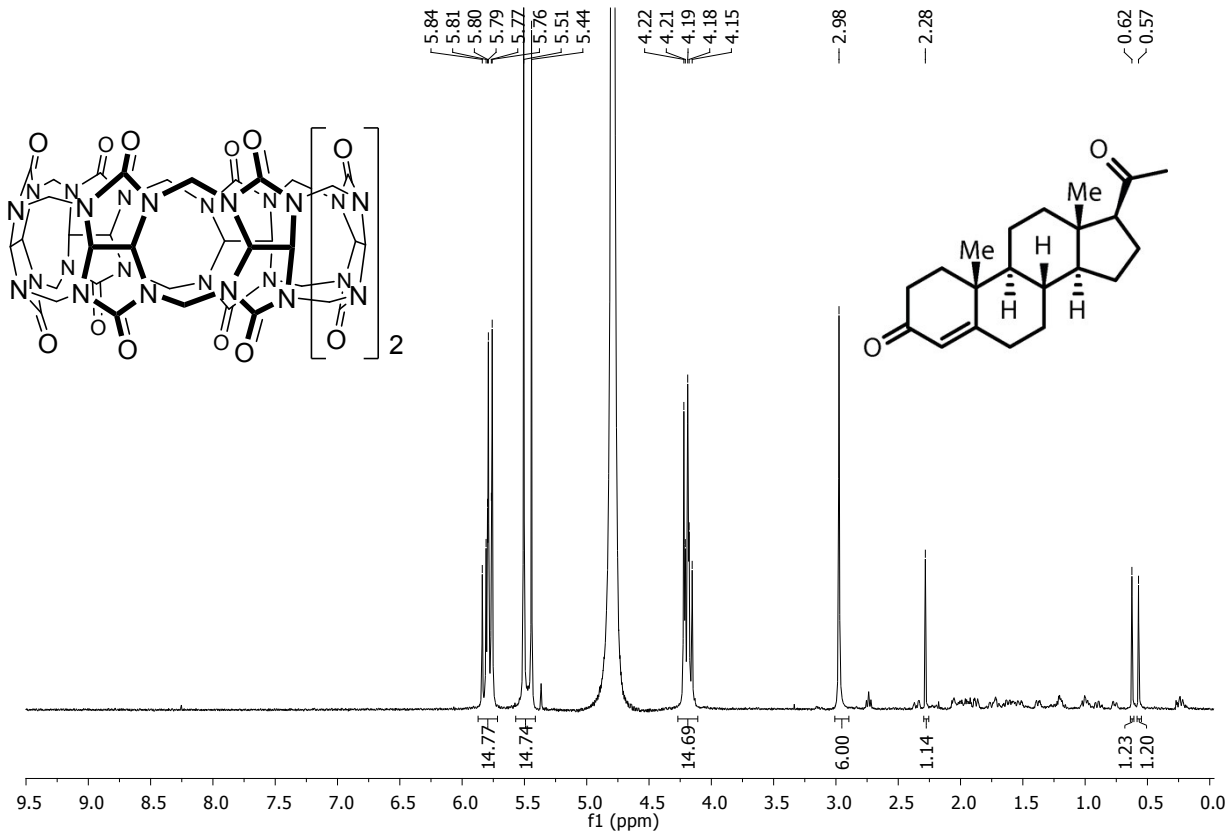

Fig. S34: ^{1}H-NMR (500 MHz, D_2O) spectrum of the CB7/progesterone complex. All signals in the region of 0.57 to 2.28 can be referred to progesterone. For the concentration determination progesterone only the signal from 0.57 to 0.62ppm and 2.28ppm were integrated and used. The signals in in the region 4.15 to 4.23ppm and 5.47 to 5.84ppm can be referred to CB7, they were all used for the concentration determination of CB7. The signal at 3.08ppm can be referred to dimethyl sulfone, which was used as a Proton reference for the concentration determination of all compounds.

Table S5: Calculation of the concentration of CB7 (top) and progesterone (bottom) via the received Integrals from **Fig. S34**.

species	integral	protons	norm. integral	divisor	conc. [mM]
DMS	6.00	6.0	1.00000		1.00000
CB7-1	14.69	14.0	1.04929	0.95303	1.04929
CB7-2	14.74	14.0	1.05286	0.94980	1.05286
CB7-3	14.77	14.0	1.05500	0.94787	1.05500
CB7-Mean					1.05238
CB7-StDev					0.00289

species	integral	protons	norm. integral	divisor	conc. [mM]
DMS	6.00	6.00	1.00000		1.00000
progesterone	1.20	3.00	0.40000	2.50000	0.40000
progesterone	1.23	3.00	0.41000	2.50000	0.40000
progesterone	1.14	3.00	0.38000	2.63158	0.38000
progesterone-Mean					0.39333
progesterone-StDev					0.00943

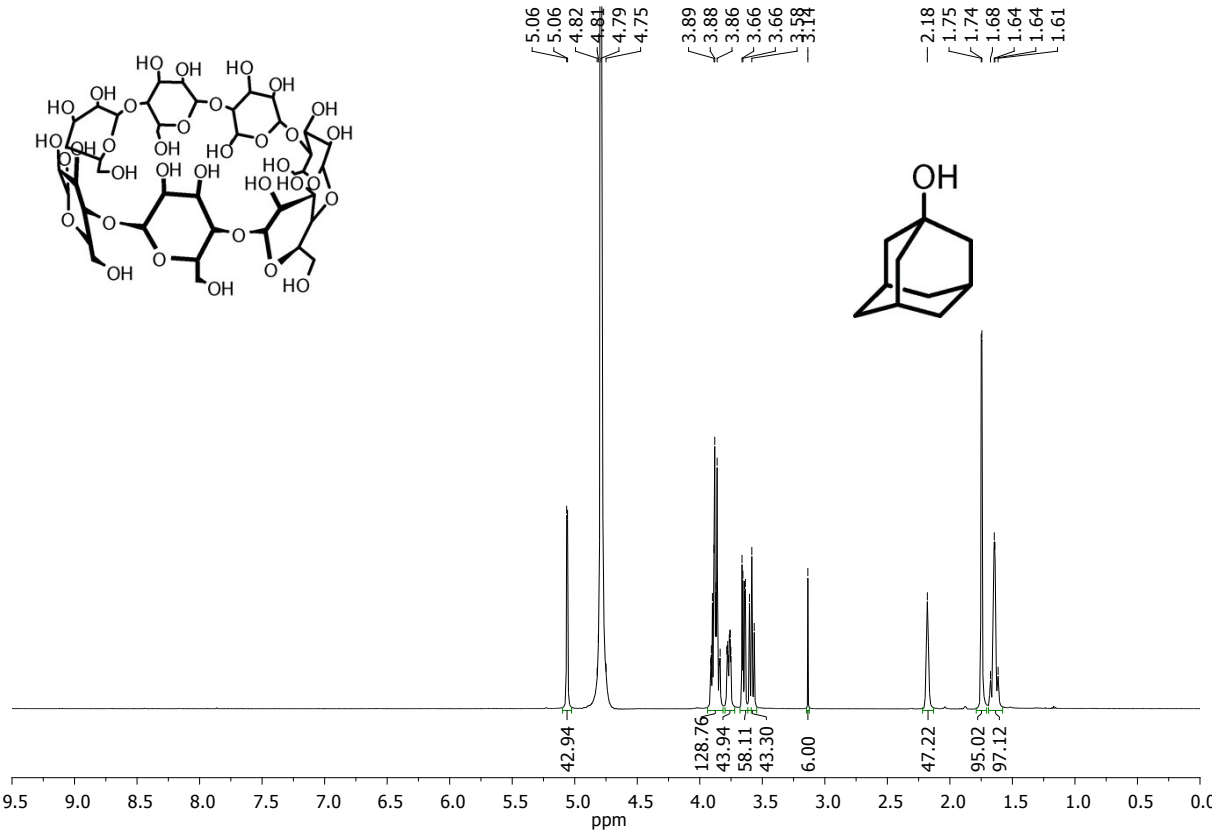

Fig. S35: ^{1}H-NMR (500 MHz, D_2O) spectrum of the β-CD⊃1-adamantanol complex. All signals in the region of 1.61 to 2.18 ppm can be referred to 1-adamantanol, the were all used for the concentration determination of 1-adamantanol. The signals in in the region 3.66 to 3.89 ppm and 4.75 to 5.06 ppm can be referred to β-CD, they were all used for the concentration determination of β-CD. The signal at 3.14ppm can be referred to dimethyl sulfone, which was used as a proton reference for the concentration determination of all compounds.

Table S6: Calculation of the concentration of CB[7] (top) and progesterone (bottom) via the received integrals from **Fig. S35**.

species	integral	protons	norm. integral	divisor	conc. [mM]
DMS	6	6	1.00000		1.00000
β-CD 1	43.3	7	6.18571	0.16166	6.18571
β-CD 2	43.23	7	6.17571	0.16192	6.17571
β-CD 3	43.94	7	6.27714	0.15931	6.27714
β-CD 4	129.45	21	6.16429	0.16222	6.16429
β-CD 5	42.94	7	6.13429	0.16302	6.13429
β-CD-Mean					6.18743
β-CD-StDev					0.05373

species	integral	protons	norm. integral	divisor	conc. [mM]
DMS	6	6	1.00000		1.00000
AdOH-1	97.12	6	16.18667	0.06178	16.18667
AdOH-2	95.02	6	15.83667	0.06314	15.83667
AdOH-3	47.22	3	15.74000	0.06353	15.74000
AdOH-Mean					15.96333
AdOH-StDev					0.235002

6 References

(1) Karásek, P.; Planeta, J.; Roth, M., *J. Chem. Eng. Data* **2008,** *53* (3), 816-819.
(2) Bendeby, B.; Kenne, L.; Sandström, C., *J. Incl. Phenom. Macrocycl. Chem.* **2004,** *50* (3), 173-181.
(3) https://www.drugbank.ca/drugs/DB00812 PBZ. https://www.drugbank.ca/drugs/DB00812 (accessed 2019.12.02).
(4) Lazar, A. I.; Biedermann, F.; Mustafina, K. R.; Assaf, K. I.; Hennig, A.; Nau, W. M., *J. Am. Chem. Soc.* **2016,** *138* (39), 13022-13029.
(5) Pilling, M. J., *Low-temperature combustion and autoignition*. Elsevier: 1997; Vol. 35.
(6) Wang, C.; Perumalla, S. R.; Lu, R.; Fang, J.; Sun, C. C., *Cryst. Growth Des.* **2016,** *16* (2), 933-939.
(7) Janoschka, T.; Martin, N.; Hager, M. D.; Schubert, U. S., *Angew. Chem. Int. Ed.* **2016,** *55* (46), 14427-14430.
(8) Schalley, C. A., *Analytical Methods in Supramolecular Chemistry*. Wiley: Weinheim, 2012.
(9) Lakowicz, J. R., *Principles of Fluorescence Spectroscopy*. 3rd ed.; Springer: 2007.
(10) Maes, V.; Engelborghs, Y.; Hoebeke, J.; Maras, Y.; Vercruysse, A., *Mol. Pharmacol.* **1982,** *21* (1), 100-107.
(11) Dotsikas, Y.; Kontopanou, E.; Allagiannis, C.; Loukas, Y. L., *J. Pharm. Biomed. Anal.* **2000,** *23* (6), 997-1003.
(12) Masson, E.; Raeisi, M.; Kotturi, K., *Isr. J. Chem.* **2018,** *58* (3-4), 413-434.
(13) Marquez, C.; Nau, W. M., *Angew. Chem. Int. Ed.* **2001,** *40* (17), 3155-3160.
(14) Marquez, C.; Hudgins, R. R.; Nau, W. M., *J. Am. Chem. Soc.* **2004,** *126* (18), 5806-5816.
(15) Zheng, X.; Li, Z.; Podariu, M. I.; Hage, D. S., *Anal. Chem.* **2014,** *86* (13), 6454-60.